IEEE Access
Multidisciplinary | Rapid Review | Open Access Journal

Received November 4, 2018, accepted November 16, 2018, date of publication November 26, 2018,
date of current version December 27, 2018.

Digital Object Identifier 10.1109/ACCESS.2018.2883308

A Simple Multi-Broadband Planar Antenna for LTE/GSM/UMTS and WLAN/WiMAX Mobile Handset Applications

XIAOCHENG WANG[1], YONGLE WU[2], (Senior Member, IEEE), WEIMIN WANG[1], AND AHMED A. KISHK[3], (Fellow, IEEE)

[1]Beijing Key Laboratory of Work Safety Intelligent Monitoring, School of Electronic Engineering, Beijing University of Posts and Telecommunications, Beijing 100876, China
[2]State Key Laboratory of Information Photonics and Optical Communications, School of Electronic Engineering, Beijing University of Posts and Telecommunications, Beijing 100876, China
[3]Department of Electrical and Computer Engineering, Concordia University, Montreal, QC H3G1M8, Canada

Corresponding author: Yongle Wu (wuyongle138@gmail.com)

This work was supported in part by the National Natural Science Foundations of China under Grants 61671084 and 61821001, in part by the Guangzhou Major Projects of Industrial Technology of China (Research and Development of Large-Scale Multi-beam Antenna Array for 5G Massive MIMO Communication), and in part by the Fund of State Key Laboratory of Information Photonics and Optical Communications, Beijing University of Posts and Telecommunications, China, under Grant IPOC2017ZR06.

ABSTRACT A simple compact low-profile multi-broadband planar antenna is proposed in this paper for LTE/GSM/UMTS and WLAN/WiMAX mobile handset applications. The proposed antenna covers multiple broad frequency bands including LTE700, GSM850, GSM900, DCS/PCS/UMTS, WLAN/WiMAX, LTE2300/2500, and LTE42/43/46. It consists of a C-shaped and U-shaped monopole on one side of a thin dielectric substrate coupled to an F-shaped strip on the other side without any lumped elements. The antenna occupies a tiny size of 15 mm × 68 mm × 0.8 mm, which makes it suitable for the popular ultra-thin smartphone applications. The antenna characteristics such as S-parameter, efficiency, peak gain, and radiation patterns are simulated by HFSS. The measured and simulated results show an excellent agreement. For more practical conditions, the antenna is stalled in a plastic housing to analyze the radiation performance. In addition, its specific absorption rate is simulated and studied by CST as well.

INDEX TERMS Broadband antenna, planar antenna, mobile applications, monopole.

I. INTRODUCTION

In the past 40 years, wireless communication technology has gone through four major wireless evolutions with an amazing speed [1]. During the period many kinds of communication standards are proposed such as LTE700 (698-787 MHz), GSM850 (824-894 MHz), GSM900 (880-960 MHz), GSM1800 (1710-1880 MHz), GSM1900 (1850-1990 MHz), UMTS (1920-2170 MHz), LTE2300 (2300-2400 MHz), LTE2500 (2500-2690 MHz) and so on. As the 5G (fifth generation) era is getting closer and closer, some frequency bands are also needed to be covered for the near future such as LTE42/43/46 (3400-3800 MHz, 5150-5195 MHz) [2], [3]. Therefore, the multiband internal antennas will be necessary for state-of-the-art 'smart phones'. In addition, the narrow frame of mobile phones has become a universal requirement of aesthetic needs. Therefore, antennas for mobile phones are required to be compact and low-profile as well. Accordingly, it is a challenge to design antennas to cover multiband especially for low-band in a minimal space.

To broaden the antenna bandwidth to meet the diverse requirements of state-of-the-art ''smart-phones'' in a limited space, lots of efforts have been delivered in the past years. Some methods have been proposed, such as reconfigurable technique [4], [5], lumped-elements or matching networks [6]–[9], coupled-feed antennas [10]–[12], and hybrid multi-mode antennas [13]–[15]. Meanwhile, many kinds of antennas with small size and multiband performance are also described, such as the loop antennas [3], [16], the monopole antennas with multiple branches [17]–[25], and the Inverted-F antennas [26], [27]. Requirements of WWAN/LTE are satisfied in [3] and [16] with loop antennas. A balanced mode for a parasitic element was first reported in [3], and through the combination of balanced and unbalanced modes, the six-mode loop antenna in [3] can cover both traditional octa-band and the LTE42/43/46 bands. However, loop antennas for mobile phone applications always show a 3-D structure, compared to the planar ones, which is not suitable enough for recent ultra-slim handsets. Generally speaking,

reconfigurable antennas can be very compact [4], [5]. In [4], the antenna occupies only 35.5 mm × 13.5 mm. By adjusting the different states of the p-i-n diode, the coupling between two primary strips can be controlled. In this way, the antenna in [4] can also cover octa-band. Unfortunately, using PIN diodes unavoidably makes the antenna structure more complicated. For the antennas with lumped-elements [6]–[9], they have the similar problem with reconfigurable ones. By loading a chip inductor to form a parallel resonant, the proposed antenna in [6] can meet the requirements of LTE/WWAN operation including LTE700 with a small clearance of 40 mm × 15 mm. But the complex structure with lumped elements makes the fabrication process complicated.

Owing to the simplicity and the compactness of the structure, the planar monopole antennas are easy to fabricate in ultra-slim mobile phones. Meanwhile, monopole antennas can easily be multi-band, which can be achieved by implementing multiple resonant modes [17]–[25]. In [17], the antenna consisted of a coupled line and two branches that can cover octa-band (704-960 MHz, 1710-2690 MHz) for WWAN/LTE using the 0.25, 0.5, and 0.75 λ modes. In [19], depending on the double-layer coupling structure, the designed antenna can cover three broad bands (790-1061 MHz, 1650-2775 MHz, 3132-6382 MHz) in a narrow space (60 mm × 15 mm) by using multiple branches without any lumped elements. It is a great achievement, except for the LTE700 that cannot be covered. Actually, few designs can cover LTE/GSM/UMTS including LTE700 as well as WLAN/WiMAX bands in one antenna. The antenna in [24] covers the whole band relying on the coupling among multiple strips, but the structure seems to be very complicated. Therefore, it is a challenge to design an antenna with simple structure meeting both the requirements of LTE/GSM/UMTS and WLAN/WiMAX operations.

To solve this problem, we propose a multi-broadband planar monopole antenna. It can meet the requirements of LTE/GSM/UMTS and WLAN/WiMAX including LTE700 with a low-profile (15 mm). Furthermore, the proposed antenna has a straightforward structure, which only consists of a C-shaped strip, and a U-shaped monopole coupled to an F-shaped strip in the opposite layer. In addition, any lumped elements are not used. From the measured results, we can observe that the −6 dB impedance bandwidths are 348 MHz (698-1046 MHz) at low-band and 1085 MHz (2703-1618 MHz), 1359 MHz (3018-4377 MHz), 1303 MHz (4697-6000 MHz) at the upper-band.

The configuration of the antenna is described in Section II. The working principle is investigated in Section III, and the measured results and discussion are presented in Section IV.

II. ANTENNA CONFIGURATION

The proposed antenna consists of a C-shaped and U-shaped monopole coupled to an F-shaped strip connected with the ground in the bottom layer (opposite side of the substrate). The configuration of the antenna is illustrated in Fig. 1. The optimized values for the geometric parameters are listed in Table. 1. As depicted in Fig. 1(b), to facilitate expression, we have defined some branches. A 0.8-mm-thick FR4 substrate is served as the system circuit board, whose relative

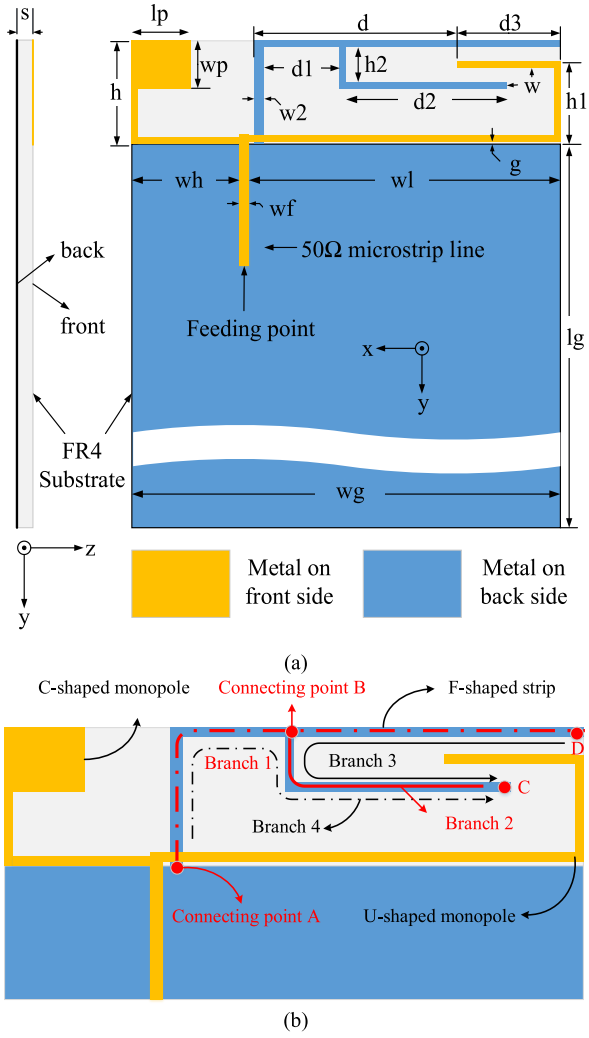

FIGURE 1. Configuration of the proposed multi-broadband planar antenna. (a) Geometry of the proposed antenna. (b) Annotation of the antenna structure. Branches 1-4 are AD, BC, DC, and AC, respectively.

TABLE 1. Optimized geometric parameters for the multi-broadband planar antenna.

Parameter	Value(mm)	Parameter	Value(mm)
lp	9.5	wp	7
d1	13	d2	26.8
d3	17	h	15
h1	12	h2	5
wf	1.5	wg	68
w2	1.5	w	1
wh	15	wl	51.5
lg	121	g	0.4
s	0.8	d	33.5

permittivity and loss tangent are 4.4 and 0.024, respectively. For 5.5-inch mobile phone screen, the dimension of the board is 68 mm × 136 mm × 0.8 mm. On the bottom layer, the main ground is printed with a size of 68 mm × 121 mm. A 50 Ω micro-strip line feed with a width of 1.5 mm is printed on the top layer, and it is connected to an SMA on the opposite layer through a via-hole. Fig. 2 shows the photos of the fabricated antenna.

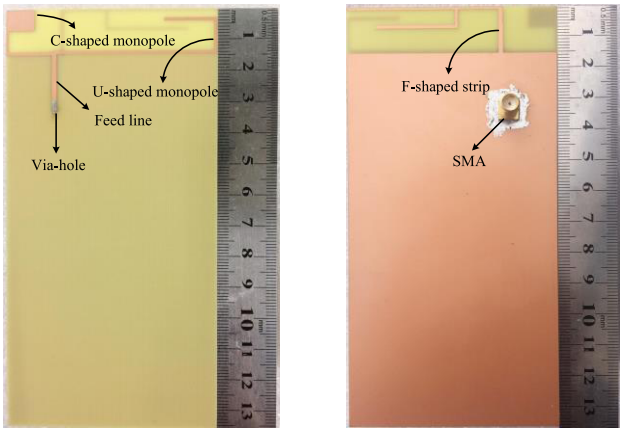

FIGURE 2. Photos of the multi-broadband planar antenna. (a) Front view. (b) Back view.

According to the measured results, the proposed multi-broadband planar antenna can respectively cover the −6 dB impedance bandwidth of 348 MHz (698-1046 MHz) for LTE700/GSM850/GSM900; 1085 MHz (1608-2703 MHz) for DCS/PCS/UMTS/LTE2300/LTE2500, WLAN 2.4 GHz band and WiMAX 2.5 GHz band; 1359 MHz (3018-4377 MHz) for LTE42/LTE43 and WiMAX 3.5 GHz band, and 1303 MHz for LTE46 or LTE-U/LTE-LAA [28]. In addition, for more practical conditions, a plastic housing (relative permittivity 3.0, loss tangent 0.02) with a dimension of 70 mm × 140 mm × 10 mm and a thickness of 1 mm was 3D-printed to enclose the system circuit. The proposed antenna was simulated and studied using the commercial software Ansoft HFSS. Meanwhile, the SAR was also simulated and calculated with CST.

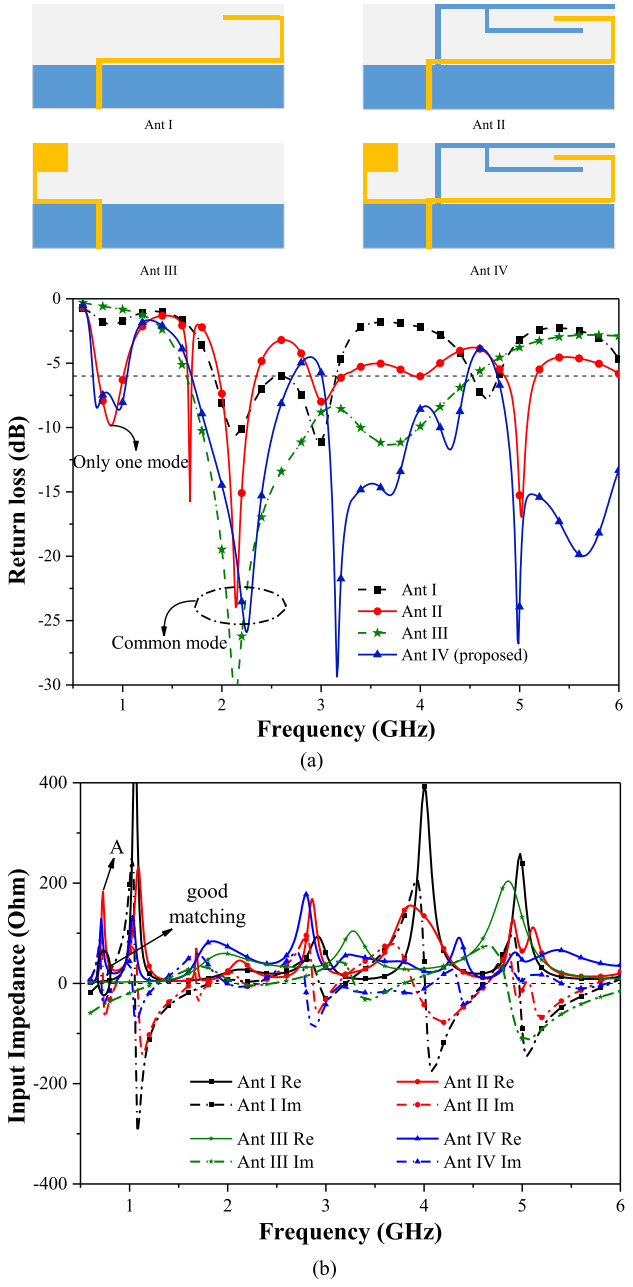

FIGURE 3. Simulated return loss and the input impedance of Ant I, Ant II, Ant III, and Ant IV. (a) Simulated return loss. (b) Simulated input impedance.

III. WORKING PRINCIPLES

A. OVERVIEW OF RESONANT MODES

To discuss the working principles of the proposed antenna, we divide the design into four parts. Ant I consists of the U-shaped monopole. Ant II is formed by the U-shaped and F-shaped strip on the other side. Ant III consists of the C-shaped monopole. Ant IV is the combination of Ant II and Ant III presenting the overall proposed antenna.

As shown in Fig 3, the results of the simulated S-parameter and input impedance are compared with the four mentioned above antennas. From Fig. 3(a), it can be observed that Ant I resonates at around 900 MHz, 2150 MHz, 3000 MHz, and 4660 MHz in sub-6 GHz frequency band. Note that the total length of the U-shaped monopole is around 81.4 mm, and it is about a quarter of a wavelength at 900 MHz. The 3000 MHz and 4669 MHz are high order resonant modes, which are 3 f_0 and 5 f_0 (f_0 is the 900 MHz base frequency), respectively. For the mode at 2150 MHz, it can be observed from Fig.3(a) that four antennas resonant near this mode. This is mainly due to the influence of the PCB board. As for Ant I, in the lower band, only one resonant mode at around 900 MHz, and the matching is poor due to its very high real part impedance. Generally, to cover frequency bands of LTE700 and GSM850/900, we usually need at least

two resonant modes. Therefore, we design an F-shaped strip on the bottom coupling with the U-shaped monopole.

However, from the simulated S-parameters results of Ant II in the lower band, there is still only one resonant mode that can be observed in Fig. 3(a). Meanwhile, from the simulated input impedance results of Ant II, a new resonant mode 'A' is generated at around 730 MHz, which rarely has impedance matching at this point. Therefore, the new resonant mode 'A' is already generated by the coupling between U-shaped monopole and F-shaped strip. It is mainly because the dual-layer coupling structure provides an additional capacitance to compensate the high input reactance of the planar monopole antenna. Under these circumstances, for branches with certain lengths, a lower resonance will be generated [23]. Owing to the poor matching, mode 'A' is hidden by the original 900 MHz resonant mode. Therefore, it cannot be observed on the curve of the simulated S-parameters results. The next step is to make the matching better at around 730 MHz.

On the other hand, note that Ant II has a few resonances at around 1680/2150/3020/4000/5020 MHz in upper band. However, they do not have a good match so that the desired frequency bands cannot be covered. Therefore, to meet the requirements of LTE 42/43, a C-shaped monopole is introduced in Ant III. As shown in Fig. 3(a), Ant III resonates at around 2140 MHz and 3700 MHz, and the −6 dB impedance bandwidth is satisfied. By adding the C-shaped monopole, Ant IV is formed. As depicted in Fig. 3(b), a better impedance matching is achieved in the circular area. Therefore, the resonant mode 'A' can be seen in Fig. 3(a) at around 730 MHz to broaden the impedance bandwidth for the lower band, which will be later illustrated by the surface current distribution in the next subsection. For the upper band, two new resonant modes are introduced respectively at around 3700 MHz and 5600 MHz by means of the C-shaped monopole. Therefore, the requirements of LTE42/43/46 can be satisfied. In addition, due to the change of the input impedance, the addition of the C-shaped monopole also improves impedance matching for the original resonant modes, thus increasing impedance bandwidth to achieve broadband performance.

B. MULTIPLE RESONANT MODES ANALYSIS

In this study, the radiator mainly relies on the coupling between the U-shaped and the F-shaped strip on the other side. As mentioned above, the dual-layer coupling structure provides an addition capacitance for compensating the high input reactance. So we cannot determine the working mode through the length of branches in this study. Precise values of parameters have to be chosen through optimization. So we mainly investigate the working principles through the simulated surface current distributions. As depicted in Figs. 4(a)-(h) according to the resonant frequencies. In addition, the directions of currents are depicted with black arrows. Meanwhile, the current maximum and nulls are both marked with red and black points, respectively. It is clear that at all frequencies, the current is zero at the end of any radiating part as this an enforcing of the boundary conditions.

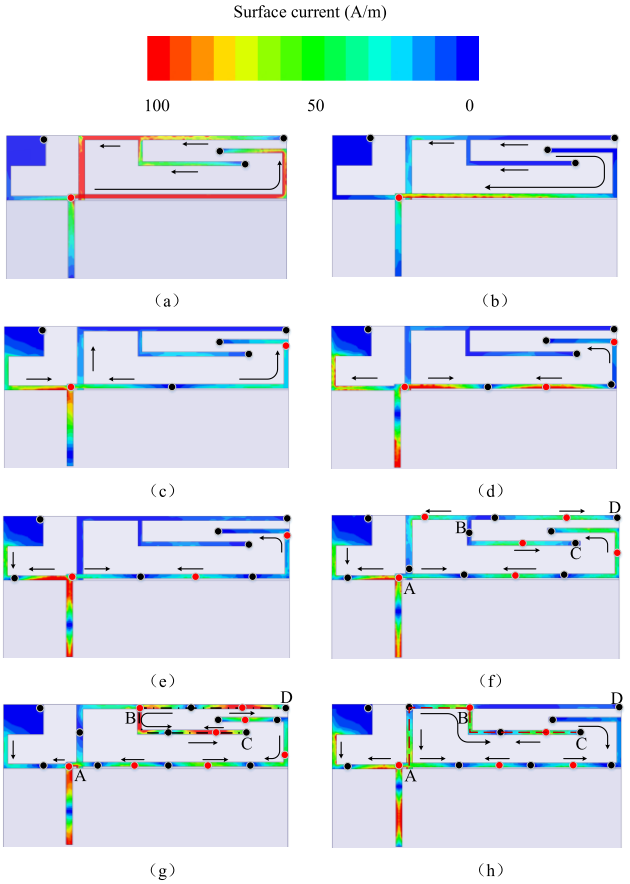

FIGURE 4. Simulated surface current distributions at different frequencies. (a) 740 MHz. (b) 960 MHz. (c) 2240 MHz. (d) 3160 MHz. (e) 3700 MHz. (f) 4300 MHz. (g) 4980 MHz. (h) 5600 MHz.

As shown in Fig. 4(a), the surface current concentrates mostly on the U-shaped monopole and F-shaped strip at 740 MHz. The current on the F-shaped strip is mainly generated by electromagnetic coupling with a U-shaped monopole. It indicates that they together generate the 740 MHz resonant mode. To investigate the working principle of the 740 MHz mode, an abstract current path model is depicted in Fig. 5. I_u and I_f are the currents distributed on the U-shaped and the F-shaped strip, respectively. α and β are the coupling coefficient between I_u and I_f. According to the directions of currents, I_f can be written as

$$I_f = I_u(\alpha + \beta) \tag{1}$$

As depicted in Fig. 5, the U-shaped and F-shaped strips are forming a current loop with a capacitive loading due to the overlapped parts of them. Thus, the 740 MHz mode is mainly coming from the loop, which relies on the coupling between the F-shaped and U-shaped strip.

In Fig. 4(b), it can be seen that the surface current is mainly distributed on the U-shaped monopole. There is one current null and one current maximum on the U-shaped monopole. Therefore, it shows a monopole-like λ/4 mode that is mostly introduced by the U-shaped monopole at 960 MHz.

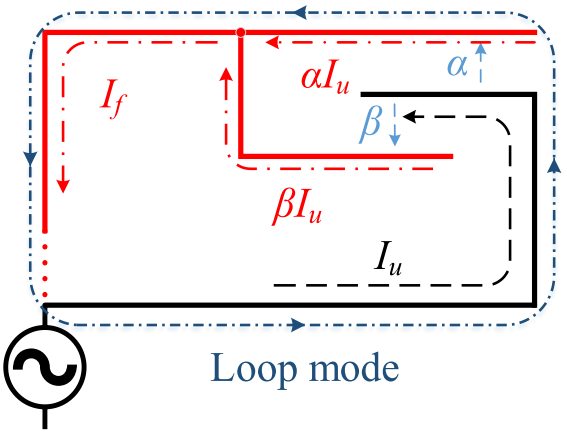

FIGURE 5. Current path model for the 740 MHz mode. (The directions of currents of U-shaped monopole and F-shaped strip are depicted by black and red arrows, respectively).

From the surface current distribution depicted in Fig. 4(c) at 2240 MHz, it can be seen that two current maximums exist respectively at the start and the medium of the U-shaped monopole. Meanwhile, as marked with black points, two current nulls appear. Therefore, it is a monopole-like 3λ/4 mode generated by the U-shaped monopole at 2240 MHz. On the other hand, it is clearly seen that the C-shaped monopole works at a monopole-like λ/4 mode because a null and a maximum appear respectively at the end and the start along the path. Based on the above analysis method, from Fig. 4(d), a λ/4 mode is also generated by the C-shaped monopole at 3160 MHz. In addition, the U-shaped monopole works at a monopole-like 5λ/4 mode because it has three current nulls together with three current maximum distributing from the start to the end.

According to the above analysis of Figs. 4(e)-(h), the C-shaped works at a monopole-like 3λ/4 mode at 3700 MHz, 4300 MHz, 4980 MHz, and 5600 MHz, but weaker at 4980 MHz. In addition, a monopole-like 5λ/4 mode is generated by the U-shaped monopole in Fig. 4(e), (f). Meanwhile, a monopole-like 7λ/4 mode is generated by that in Fig. 4(g), (h). From the current distribution depicted in Fig. 4(f)-(h), there is strong current distributing on the F-shaped strip. Next, we will focus on it. As shown in Fig. 4(f), it can be seen that three current nulls and maximums appear together on Branch 1(A-B-D), which corresponds to a 2λ mode. But it cannot radiate energy effectively because of the existence of two equal-amplitude but antiphase currents. From Fig. 4(g) we can observe that the surface current direction at junction point B is identical. In addition, the strip B-C and strip B-D both have two nulls and two maximums along with the path. It corresponds to the Branch 3 they form together, and it offers a dipole-like 3λ/2 mode. The similar phenomenon is also presented in [21]. For surface current distribution of F-shaped strip in Fig. 4(h), there is strong energy distributing from connecting A to C. As depicted from the number of current null and maximum, the Branch 4 works at a monopole-like 7λ/4 mode.

The above is a possible explanation, but a hidden contribution is coming from the horizontal part of the strip parallel to the edge of the ground plane. This form strong fringing fields between the strip and the ground plane edge causing radiation that is mainly z-polarized, which is very strong and dominate the radiation in all bands.

According to the above analysis of the surface current distributions on the proposed antenna, we can conclude that it works at many different resonant modes of loop mode at 740 MHz, monopole-like λ/4, 3λ/4, 5λ/4, 7λ/4 modes, and the dipole-like 3λ/2 mode. Nearly every resonant mode is combined with multiple modes. Thus, it makes important contributions to the multi-broadband performance of the proposed antenna. Also, the fringing fields contribute strongly to the second polarization as mentioned above.

IV. SIMULATED AND MEASURED RESULTS

The proposed broadband antenna is fabricated according to the dimensions depicted in Fig. 1, and its photos are shown

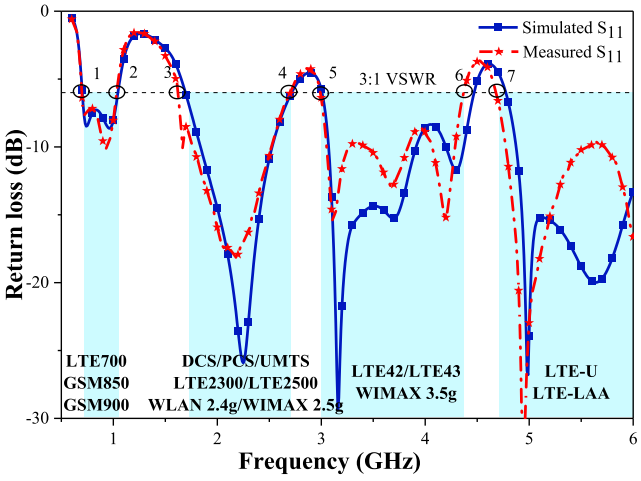

FIGURE 6. Measured return loss compared to simulated result for the proposed antenna. Points 1-7 are 698 MHz, 1046 MHz, 1618 MHz, 2703 MHz, 3018 MHz, 4377 MHz and 4697 MHz, respectively.

FIGURE 7. Prototype of the multi-broadband planar antenna with the plastic housing.

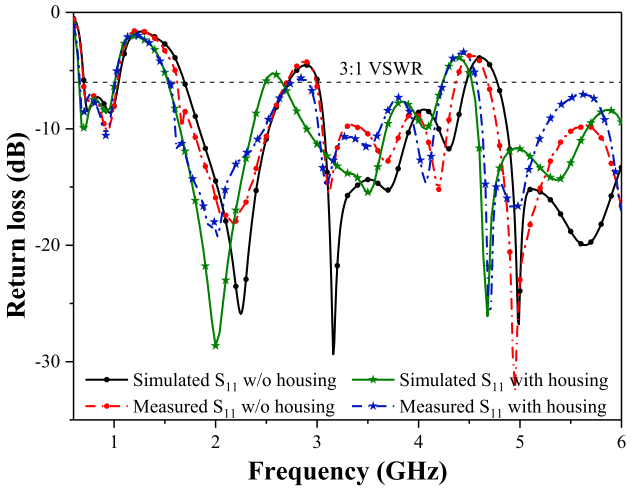

FIGURE 8. Comparison of the simulated and measured S-parameters of the proposed antenna with and without the housing.

in Fig. 2 including the front and back sides. The S-parameters are measured by an R&S ZVA 8 vector network analyzer. The radiation patterns, efficiency, and peak gain are obtained in a SATIMO microwave anechoic chamber. In addition, the SAR (specific absorption rate) is also simulated and studied by CST.

Fig. 6 shows the comparison between simulated and measured S_{11}, and the results are in good agreement. The measured −6 dB impedance bandwidths are 348 MHz (698-1046 MHz) at lower-band and 1085 MHz (2703-1618 MHz), 1359 MHz (3018-4377 MHz), 1303 MHz (4697-6000 MHz) at upper-band (Consider that practical application and restriction of experimental conditions, the curve does not include the frequency over 6 GHz). According to the measured and simulated results, the broadband performance is achieved. So it can ultimately meet the requirements of LTE/GSM/UMTS and WLAN/WiMAX handset applications. As shown in Fig. 7, the plastic housing is fabricated using 3D-printing to enclose the system circuit for more realistic conditions. In order to make a precise comparison, Figure. 8 shows the simulated and measured S-parameter results of the proposed antenna with and without an enclosure. When the housing exists, for both simulated and measured results, it can be observed that the resonances are slightly shifted to lower frequencies. It is mainly due to that the antenna and housing together form a new radiator. In this case the antenna can still meet the requirement as far as frequency band is concerned.

The radiation patterns are simulated and measured at 740 MHz, 2240 MHz, 3500 MHz, and 5600 MHz to represent the performance both in low and high bands. The results are demonstrated in Fig. 9. Their radiation performance is

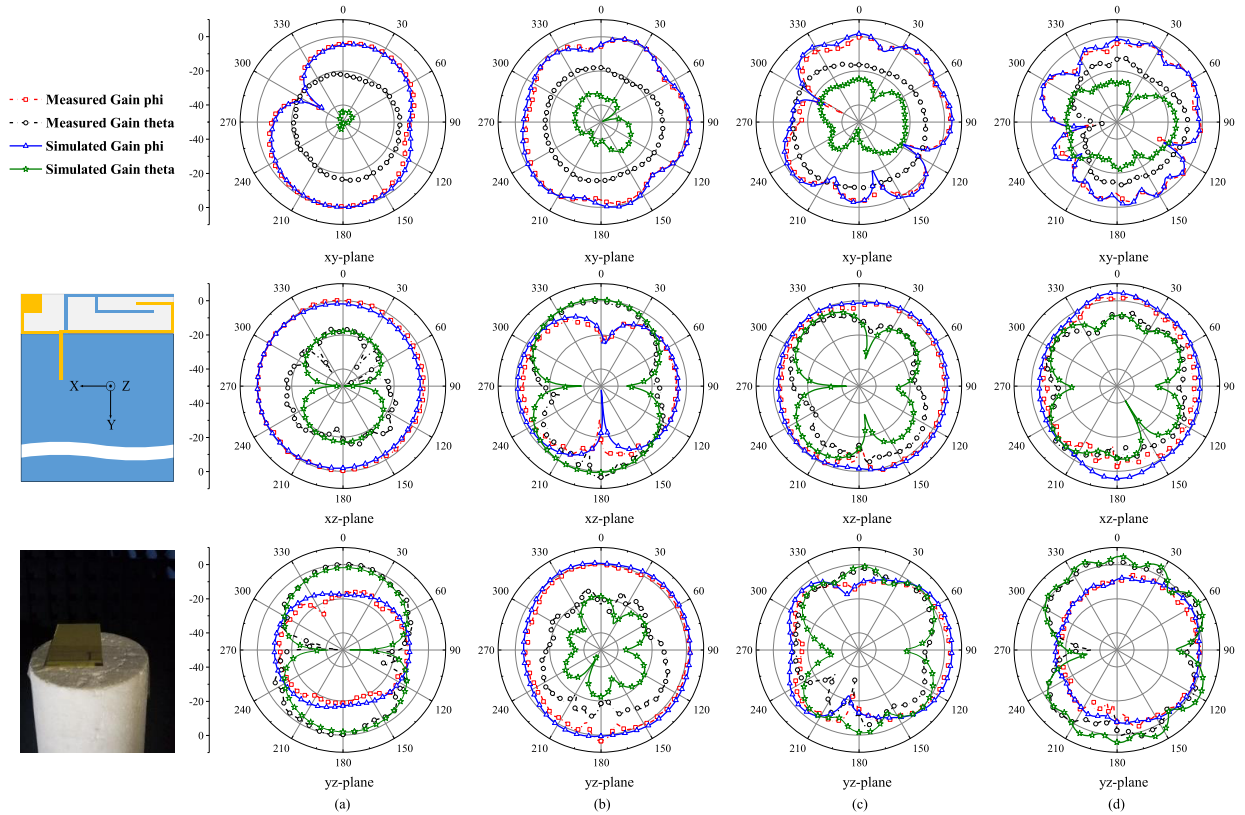

FIGURE 9. Simulate and measured radiation patterns of proposed antenna in three principal planes at different frequencies. (a) 740 MHz. (b) 2240 MHz. (c) 3500 MHz. (d) 5600 MHz.

described including both E_ϕ and E_θ in three planes: x-z, y-z, and x-y. As depicted in Figs. 9(a) and (b), the results show an omnidirectional dipole-like performance in x-z and y-z plane at every investigated frequency, which indicates that the proposed antenna is suitable for today's mobile communications system. The E_θ in the x-y plane does not show a satisfactory agreement between the simulated and measured results, which is mainly due to the deviation of the production and measurement.

The peak gain and efficiency are both measured in a SATIMO microwave anechoic chamber, and the results are plotted in Figs. 10(a) and (b), respectively. For more practical situations, the proposed antenna with housing is also measured and compared. From Figs. 10(a) and (b), the results show that without housing, the peak gain is 0.4-2.8 dBi in 0.7-1.0 GHz band, 1.9-4.3 dBi in 1.7-2.7 GHz band, 2.4-4.4 dBi in 3.0-4.1 GHz band, and 4.3-5.6 dBi in 4.9-6.0 GHz band, respectively. When the antenna is installed in the plastic enclosure, the peak gain decreases slightly, while in upper-band it will be severely affected. As depicted in Fig. 10(a) and (b), it can be observed that the efficiency varies between 50% and 87% for the above mentioned four frequency bands, and the antenna housing brings about similar affection to efficiency and peak gain. Although there is some deterioration on the boundary of the desired frequency, it is acceptable in practical conditions.

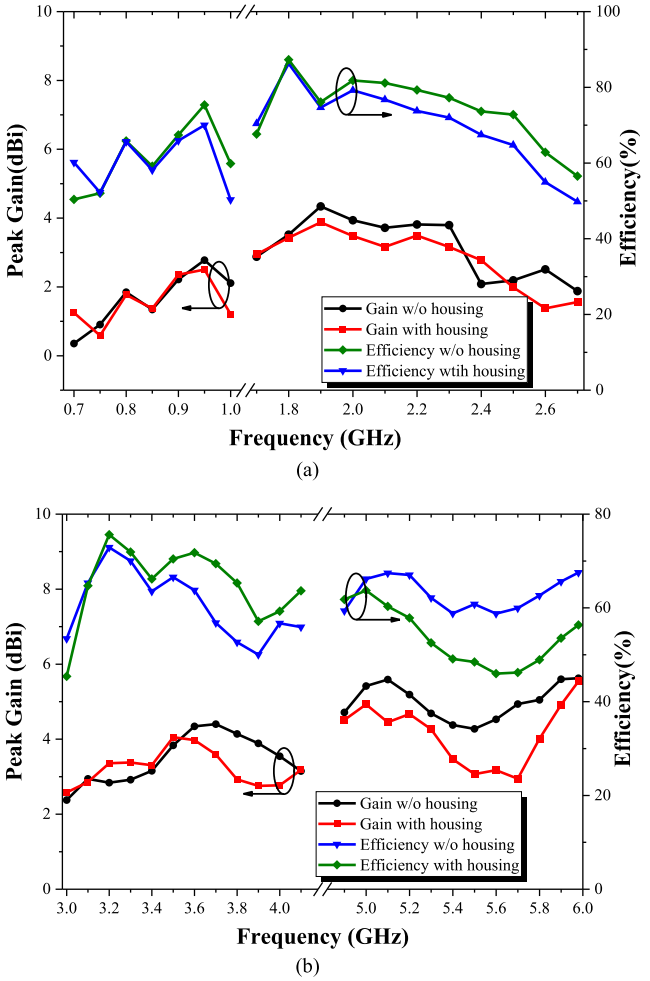

FIGURE 10. Measured peak gain and antenna efficiency of the multi-broadband planar antenna with and without housing. (a) 0.7-2.7 GHz band. (b) 3.0-4.1 GHz and 4.9-6.0 GHz bands.

The SAR is also simulated and studied with CST, and the head model is provided by the software. As illustrated in Fig. 11, the proposed antenna is placed at the bottom of the system circuit board to decrease the SAR [23]. The distance between the board and the head phantom ear is 5 mm, and the board is inclined to the vertical line by 60 degrees. In this study, the simulated input power is 21 dBm at 740 MHz, 1795 MHz, 1920 MHz, 2045 MHz and 2350 MHz, 24 dBm at 859MHz, 925 MHz, 5200 MHz and 5800 MHz, and 23 dBm at 3500 dBm [23]. For 10-g head tissue, the limit value is 2.0 W/kg. From the simulated results listed in Table. 2, we can observe all the SAR values are below the limitation, corresponding to a suitable performance for mobile phone applications.

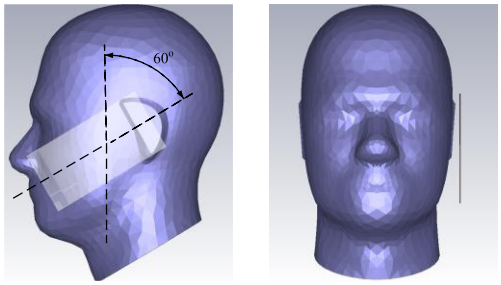

FIGURE 11. Head phantom simulation model provided by CST with the proposed antenna placed near to the ear at an inclined angle.

TABLE 2. Simulated SAR values for 10-g head issue.

Frequency (MHz)	740	859	925	1795	1920
Input power (Watt in dBm)	21	24	24	21	21
Return loss (dB)	3.61	7.21	5.75	5.41	5.72
10-g SAR (W/Kg)	0.26	0.90	0.83	0.18	0.19
Frequency (MHz)	2045	2350	3500	5200	5800
Input power (Watt in dBm)	21	21	23	24	24
Return loss (dB)	6.45	16.17	7.56	18.30	7.19
10-g SAR (W/Kg)	0.19	0.22	0.22	0.38	0.46

Table. 3 compares the proposed antennas with some recent published antennas. In the Table, the antenna dimension,

TABLE 3. Comparison of proposed antenna and reference antennas.

Ref.	Dimension (mm^3)	-6 dB Bandwidth (MHz)	Eff. (%)	Lumped element using
Proposed	68×15×0.8	698-1046 1618-2703 3018-4377 4697-6000	50-87	No
[6]	40×15×0.8	704-965 1660-2710	45-75	Yes
[9]	80×8×5.8	690-980 1630-2740	50.2-94.5	Yes
[14]	60×15×0.8	660-1065 1665-3000	42-88	No
[17]	80×6×5.8	670-1020 1650-2920	63.2-97.2	No
[19]	60×15×0.5	790-1061 1650-2775 3132-6382	60-91	No
[22]	20×15×0.8	810-980 1710-2700	41-82	No

Dimension: the size of antenna alone; Eff: the results of measured total efficiency;

frequency band, efficiency, and lumped using are provided. From the table we can observe that the antennas proposed in [9] and [17] both occupy minimal nonground height, and they both can cover octa-band for LTE/WWAN requirements. However, the antenna volume seems to be less attractive because of their 3-D structure. The antennas in [6] and [22] show a very mini volume but the efficiency cannot acquire excellent performance. Furthermore, the proposed antenna in [6] uses lumped elements to achieve better matching, which inevitably brings some difficulties to antenna manufacturing. In [22], the proposed antenna cannot meet the requirements of LTE700. Compared with the same type antennas published in [14] and [19] the proposed antenna does not have an advantage in dimension size. However, the requirements of LTE/GSM/UMTS and WLAN/WiMAX can be totally satisfied including the LTE700 with a straightforward structure, which is very important for fabricating antennas in ultra-slim mobile phones. Furthermore, any lumped elements are not used in this study.

Therefore, the proposed antenna is attractive for modern and next 5G era.

V. CONCLUSION

A compact and low-profile multi-broadband planar antenna has been proposed and studied for LTE/GSM/UMTS and WLAN/WiMAX mobile phone applications. The proposed antenna can completely satisfy the requirements of LTE700, GSM850, GSM900, DCS/PCS/UMTS, WLAN/WiMAX, LTE2300/2500 as well as LTE42/43/46 with a low-profile and a straightforward structure without any lumped elements. In addition, the radiation performances are satisfactory. The efficiency and peak gain have been found between 50% and 87%, 0.4 dBi and 5.6 dBi, respectively. Furthermore, the simulated SAR values have achieved less than 2.0 W/kg for 10-g head tissue at different frequencies. Therefore, the proposed design is suitable for now state-of-the-art ''smart phones'' and promising for modern and next 5G era.

Furthermore, there are still some defects in the design. For example, the dimension size of the antenna is a bit large. It is expected that the height of the non-ground portion can be further optimized.

REFERENCES

[1] W. Hong, ''Solving the 5G mobile antenna puzzle: Assessing future directions for the 5G mobile antenna paradigm shift,'' *IEEE Microw. Mag.*, vol. 18, no. 7, pp. 86–102, Nov. 2017.
[2] Y. Li, C.-Y.-D. Sim, Y. Luo, and G. Yang, ''12-port 5G massive MIMO antenna array in sub-6GHz mobile handset for LTE bands 42/43/46 applications,'' *IEEE Access*, vol. 6, pp. 344–354, Oct. 2017.
[3] H. Xu *et al.*, ''A compact and low-profile loop antenna with six resonant modes for LTE smartphone,'' *IEEE Trans. Antennas Propag.*, vol. 64, no. 9, pp. 3743–3751, Sep. 2016.
[4] S. W. Lee, H. S. Jung, and Y. J. Sung, ''A reconfigurable antenna for LTE/WWAN mobile handset applications,'' *IEEE Antennas Wireless Propag. Lett.*, vol. 14, pp. 48–51, Jan. 2015.
[5] H. Wang *et al.*, ''Small-size reconfigurable loop antenna for mobile phone applications,'' *IEEE Access*, vol. 4, pp. 5179–5186, Jul. 2016.
[6] Y.-L. Ban, J.-H. Chen, S. Yang, J.-L.-W. Li, and Y.-J. Wu, ''Low-profile printed octa-band LTE/WWAN mobile phone antenna using embedded parallel resonant structure,'' *IEEE Trans. Antennas Propag.*, vol. 61, no. 7, pp. 3889–3894, Jul. 2013.
[7] L.-W. Zhang, Y.-L. Ban, C.-Y.-D. Sim, J. Guo, and Z.-F. Yu, ''Parallel dual-loop antenna for WWAN/LTE metal-rimmed smartphone,'' *IEEE Trans. Antennas Propag.*, vol. 66, no. 3, pp. 1217–1226, Mar. 2018.
[8] Y.-L. Ban, C.-L. Liu, Z. Chen, J.-L.-W. Li, and K. Kang, ''Small-size multiresonant octaband antenna for LTE/WWAN smartphone applications,'' *IEEE Antennas Wireless Propag. Lett.*, vol. 13, pp. 619–622, Mar. 2014.
[9] Y. Wang and Z. Du, ''Wideband monopole antenna with less nonground portion for octa-band WWAN/LTE mobile phones,'' *IEEE Trans. Antennas Propag.*, vol. 64, no. 1, pp. 383–388, Jan. 2016.
[10] Y.-L. Ban, C.-L. Liu, J. L.-W. Li, J. Guo, and Y. Kang, ''Small-size coupled-fed antenna with two printed distributed inductors for seven-band WWAN/LTE mobile handset,'' *IEEE Trans. Antennas Propag.*, vol. 61, no. 11, pp. 5780–5784, Nov. 2013.
[11] Z. Xie, W. Lin, and G. Yang, ''Coupled-fed printed antenna for LTE mobile handset applications,'' *Microw. Opt. Technol. Lett.*, vol. 56, no. 8, pp. 1752–1756, Aug. 2014.
[12] D.-G. Kang and Y. Sung, ''Coupled-fed planar printed shorted monopole antenna for LTE/WWAN mobile handset applications,'' *IET Microw. Antennas Propag.*, vol. 6, no. 9, pp. 1007–1010, Jul. 2012.
[13] C. Deng, Y. Li, Z. Zhang, and Z. Feng, ''A novel low-profile hepta-band handset antenna using modes controlling method,'' *IEEE Trans. Antennas Propag.*, vol. 63, no. 2, pp. 799–804, Feb. 2015.
[14] C. Deng, Y. Li, Z. Zhang, and Z. Feng, ''Planar printed multi-resonant antenna for octa-band WWAN/LTE mobile handset,'' *IEEE Antennas Wireless Propag. Lett.*, vol. 14, pp. 1734–1737, Apr. 2015.
[15] J.-W. Lian, Y.-L. Ban, Y.-L. Yang, L.-W. Zhang, C.-Y.-D. Sim, and K. Kang, ''Hybrid multi-mode narrow-frame antenna for WWAN/LTE metal-rimmed smartphone applications,'' *IEEE Access*, vol. 4, pp. 3991–3998, 2016.
[16] D. Wu, S. W. Cheung, and T. I. Yuk, ''Compact 3D-loop antenna with bandwidth enhancement for WWAN/LTE mobile-phones applications,'' *IET Microw., Antennas Propag.*, vol. 11, no. 2, pp. 240–246, Jan. 2017.
[17] D. Huang, Z. Du, and Y. Wang, ''An octa-band monopole antenna with a small nonground portion height for LTE/WLAN mobile phones,'' *IEEE Trans. Antennas Propag.*, vol. 65, no. 2, pp. 878–882, Feb. 2017.
[18] T. Zhang, R. Li, G. Jin, G. Wei, and M. M. Tentzeris, ''A novel multiband planar antenna for GSM/UMTS/LTE/Zigbee/RFID mobile devices,'' *IEEE Trans. Antennas Propag.*, vol. 59, no. 11, pp. 4209–4214, Nov. 2011.
[19] H. Liu, R. Li, Y. Pan, X. Quan, L. Yang, and L. Zheng, ''A multi-broadband planar antenna for GSM/ UMTS/LTE and WLAN/WiMAX handsets,'' *IEEE Trans. Antennas Propag.*, vol. 62, no. 5, pp. 2856–2860, May 2014.

[20] C.-H. Chang and K.-L. Wong, "Small-size printed monopole with a printed distributed inductor for pentaband WWAN mobile phone application," *Microw. Opt. Technol. Lett.*, vol. 51, no. 12, pp. 2903–2908, Dec. 2009.
[21] Y. Yang, Z. Zhao, W. Yang, Z. Nie, and Q.-H. Liu, "Compact multimode monopole antenna for metal-rimmed mobile phones," *IEEE Trans. Antennas Propag.*, vol. 65, no. 5, pp. 2297–2304, May 2017.
[22] G.-H. Kim and T.-Y. Yun, "Small wideband monopole antenna with a distributed inductive strip for LTE/GSM/UMTS," *IEEE Antennas Wireless Propag. Lett.*, vol. 14, pp. 1677–1680, Mar. 2015.
[23] J. Ma, Y. Z. Yin, J. L. Guo, and Y. H. Huang, "Miniature printed octaband monopole antenna for mobile phones," *IEEE Antennas Wireless Propag. Lett.*, vol. 9, pp. 1033–1036, Oct. 2010.
[24] Y. Cui, L. Yang, B. Liu, and R. Li, "Multiband planar antenna for LTE/GSM/UMTS and WLAN/WiMAX handsets," *IET Microw., Antennas Propag.*, vol. 10, no. 5, pp. 502–506, Apr. 2016.
[25] R. Tang and Z. Du, "Wideband monopole without lumped elements for octa-band narrow-frame LTE smartphone," *IEEE Antennas Wireless Propag. Lett.*, vol. 16, pp. 720–723, Aug. 2016.
[26] Y. Liu, Y.-M. Zhou, G.-F. Liu, and S.-X. Gong, "Heptaband inverted-F antenna for metal-rimmed mobile phone applications," *IEEE Antennas Wireless Propag. Lett.*, vol. 15, pp. 996–999, 2016.
[27] J. Lee and Y. Sung, "Heptaband inverted-F antenna with independent resonance control for mobile handset applications," *IEEE Antennas Wireless Propag. Lett.*, vol. 13, pp. 1267–1270, Jun. 2014.
[28] R. Zhang, M. Wang, L. X. Cai, Z. Zheng, X. Shen, and L.-L. Xie, "LTE-unlicensed: The future of spectrum aggregation for cellular networks," *IEEE Wireless Commun.*, vol. 22, no. 3, pp. 150–159, Jun. 2015.

XIAOCHENG WANG received the B.S. degree in electromagnetic field and radio technology from Xidian University, Xi'an, China, in 2017. He is currently pursuing the M.S. degree with the Beijing University of Posts and Telecommunications. In 2017, he started his research at BUPT.

His research interests include internal antennas for 5G mobile handset applications and multi-in multi-out antenna arrays.

YONGLE WU (M'12–SM'15) received the B.Eng. degree in communication engineering and the Ph.D. degree in electronic engineering from the Beijing University of Posts and Telecommunications (BUPT), Beijing, China, in 2006 and 2011, respectively.

In 2010, he joined the City University of Hong Kong, Hong Kong, as a Research Assistant. In 2011, he joined BUPT, where he is currently a Full Professor with the School of Electronic Engineering. His research interests include microwave components, circuits, antennas, and wireless systems design.

WEIMIN WANG received the B.S. degree in communication engineering, the M.S. degree in electromagnetic field and microwave technology, and the Ph.D. degree in electronic science and technology from the Beijing University of Posts and Telecommunications (BUPT), Beijing, China, in 1999, 2004, and 2014, respectively. In 2014, she joined BUPT, where she is currently a Lecturer with the School of Electronic Engineering. Her research interests include electromagnetic field and multi-in multi-out OTA measurement.

AHMED A. KISHK received the B.S. degree in electronic and communication engineering from Cairo University, Cairo, Egypt, in 1977, the B.Sc. degree in applied mathematics from Ain-Shams University, Cairo, in 1980, and the M.Eng. and Ph.D. degrees from the University of Manitoba, Winnipeg, Canada, in 1983 and 1986, respectively. In 1981, he joined the Department of Electrical Engineering, University of Manitoba. From 1995 to 2011, he was a Professor with the University of Mississippi. Since 2011, he has been a Professor and the Tier 1 Canada Research Chair of advanced antenna systems with Concordia University, Montréal, QC, Canada. He has published over 330-refereed journal articles and 450 conference papers. He has co-authored four books and several book chapters and an Editor of three books. He holds several patents to his credit. His research interests include the areas of millimeter-wave antennas for 5G applications, analog beamforming network, dielectric resonator antennas, microstrip antennas, small antennas, microwave sensors, RFID antennas for readers and tags, multi-function antennas, microwave circuits, EBG, artificial magnetic conductors, soft and hard surfaces, phased-array antennas, reflect/transmitarray, wearable antennas, and feeds for parabolic reflectors. He was a member of the AP AdCom from 2013 to 2015 and the 2017 AP-S President. He was a Feature Articles Editor of *Antennas & Propagation Magazine* from 1993 to 2014. He was an Editor-in-Chief of the ACES Journal from 1998 to 2001. He offered several short courses in international conferences.

Dr. Kishk and his students received the Microwave Theory and Techniques Society Microwave Prize 2004 and 2013 Chen-To Tai Distinguished Educator Award from the IEEE Antennas and Propagation Society.